





REFRACTIVE INDEX BASED DETECTION WITH A HIGH SENSITIVITY BIOSENSOR ENHANCED BY GRAPHENE

¹Ahmet Murat ERTURAN , ^{2,*}Seyfettin Sinan GÜLTEKİN 

^{1,2}Konya Technical University, Engineering and Natural Sciences Faculty, Electrical and Electronics Engineering
Department, Konya, TÜRKİYE

amerturan@ktun.edu.tr, ssgultekin@ktun.edu.tr

Highlights

- A highly sensitive biosensor based on graphene has been proposed.
- The achievement of 96.2% high transmission resonance mode was made possible by the strip gap created to enhance the excitation of graphene plasmons.
- The findings indicate that when analytes with varying refractive indices are exposed to the sensor surface, the sensor's sensitivity is 6282 nm/RIU.



REFRACTIVE INDEX BASED DETECTION WITH A HIGH SENSITIVITY BIOSENSOR ENHANCED BY GRAPHENE

¹Ahmet Murat ERTURAN^{ORCID}, ^{2,*} Seyfettin Sinan GÜLTEKİN^{ORCID}

*Konya Technical University, Engineering and Natural Sciences Faculty, Electrical and Electronics Engineering
Department, Konya, TÜRKİYE*

amerturan@ktun.edu.tr, ssgultekin@ktun.edu.tr

(Received: 02.05.2024; Accepted in Revised Form: 28.07.2024)

ABSTRACT: Over the past decade, optical sensors have made significant advances. An optical sensor examines the environmental impact through the change of an optical signal and offers advantages such as low cost and label-free detection. In this study, a sensor consisting of a single graphene layer and a slit positioned on the substrate is proposed. The strip gap made to improve the excitation of graphene plasmons allowed to achieve 96.2% high transmission resonance mode. This demonstrates the ability of the sensor surface to detect changing environmental conditions. The results show that the sensitivity of the sensor is 6282 nm/RIU when the sensor surface is exposed to analytes with different refractive indices. The use of a single graphene sheet eliminates the need for a metal resonator and achieves a higher sensitivity compared to some experiments recently published in the literature. Thus, the disadvantage of significant ohmic losses in metal resonators is avoided. Furthermore, a thorough discussion of various factors, including the modification of the strip gap width on the graphene layer and electrical tunability, led to the achievement of optimal sensitivity.

Keywords: *Graphene, Biosensor, Refractive Index Sensing, Plasmonics, Metamaterials*

1. INTRODUCTION

Early diagnosis of diseases and monitor the environment has grown in importance in recent years, and biosensors have made this possible [1], [2]. Biosensors are used in the detection of disease, studying the results obtained through the influence of target biomolecules on the sensor response [3]. These measurable signals play an important role in detecting the presence of biomolecules. In recent years, optical sensors capable of making high-precision measurements have attracted great attention [4], [5], [6]. Another issue that is as important as accurate early diagnosis is that this detection can be made with high sensitivity. Metamaterial-based plasmonic biosensors have great advantages in making these sensitive measurements [7]. These structures are basically obtained by dielectric and metal layers placed on a thin metal film, and this causes the interaction of light with matter along with high-energy surface plasmons developing at the dielectric-metal interface [8]. This movement at the interface changes the behavior of light and allows biomolecules to be detected sensitively depending on the collective refractive index difference. In contrast to these advantages, the most important disadvantage of metal-structured plasmonic biosensors is their high electrical loss [9]. There are also limitations such as production difficulties, cost, volume and oxidation by interference with bioanalytes [10]. In addition, their plasmonic properties are fixed and they provide spectral responses that cannot be changed after fabrication process. For a different spectral response, the design, fabrication and characterization steps must be redone for the specific spectral range.

In recent years, graphene has become an important cornerstone for biosensing. It is very desirable due to its amazing electrical qualities, versatility, and ease of production [11], [12], [13]. Graphene consists of carbon atoms arranged in a two-dimensional structural honeycomb pattern and has the advantages of strong electrical conductivity and chemical tunability [14]. These graphene-based biosensors have been used in many sensing studies, from detection of cancer cells to DNA Detection [15], [16]. Graphene's high electron mobility and chemical tunability can be integrated into different

*Corresponding Author: Seyfettin Sinan GÜLTEKİN, ssgultekin@ktun.edu.tr

optical devices, enabling the optical sensor to operate in various spectral ranges [17]. Metals such as gold and silver are used in plasmonic sensors to improve the light-matter interaction by increasing collective electron emission at the surface; nevertheless, a significant disadvantage of these materials is their high dielectric constant and ohmic losses [18]. Surface plasmons, which are based on the optical characteristics of graphene, can be employed to offer strong confinement and large-area augmentation of electromagnetic waves in order to get over this drawback.

This article proposes a low-cost, high-performance, electrically tunable biosensor that is derived from solely graphene layers, as opposed to conventional metal-based biosensors. The graphene layer was completely coated on the substrate and a slit was formed at the center position to enhance the surface plasmon polariton effect. The impact of this slit on the transmission spectrum was investigated using numerical analysis, and a comprehensive discussion was held on the influence of graphene plasmons surrounding the slit. Furthermore, the spectrum response of the sensor at various fermi energies in the terahertz frequency range resulting from graphene's chemical tunability was investigated. In addition, the effect of the relaxation time of graphene on the spectral response is also discussed in detail. Finally, the spectrum response to environmental refractive index was investigated using bioanalytes with varying refractive indices on the sensor surface. These samples showed a high sensitivity detection capacity at 6282 nm/RIU.

2. MATERIAL AND METHODS

The proposed graphene-based biosensor's single-cell image and spectral transmission response are displayed in Figure 1. There is a single-layer graphene sheet on the SiN substrate and a longitudinal slit in the middle of the graphene sheet. The excitation of graphene plasmons is intended to be amplified around this slit. The period of the single-cell along the x and y axis was determined as $P=600$ nm. Thus, the left and right portions of the graphene slit include graphene layers that were the same height and width. The width of the graphene slit was determined as $g=60$ nm and the width of the layers around the slit along the x-axis was determined as $L=270$ nm. Numerical analysis of the single layer graphene biosensor was performed using the Finite Difference Time Domain (FDTD) method. Periodic boundary conditions were employed along the x and y axes and Perfectly Matched Layer (PML) boundary conditions were used along the z axis to determine the simulation boundary conditions. The illumination is directed at a zero-degree angle along the z-axis towards the sensor surface under x-polarized light. The transmission signal shown in Figure 1b illustrates the spectral response of the graphene-based biosensor, revealing a transmission resonance mode of 96.2% at a wavelength of 37.37 μm with a 60 nm graphene slit. The changes in both the rate and bandwidth of the transmission signal caused by the slit created on the graphene layer are discussed in the following sections. However, it should be noted that in each part where the width of the graphene slit is not specified, the width is 60 nm, which is optimized to give the result in Figure 1b.

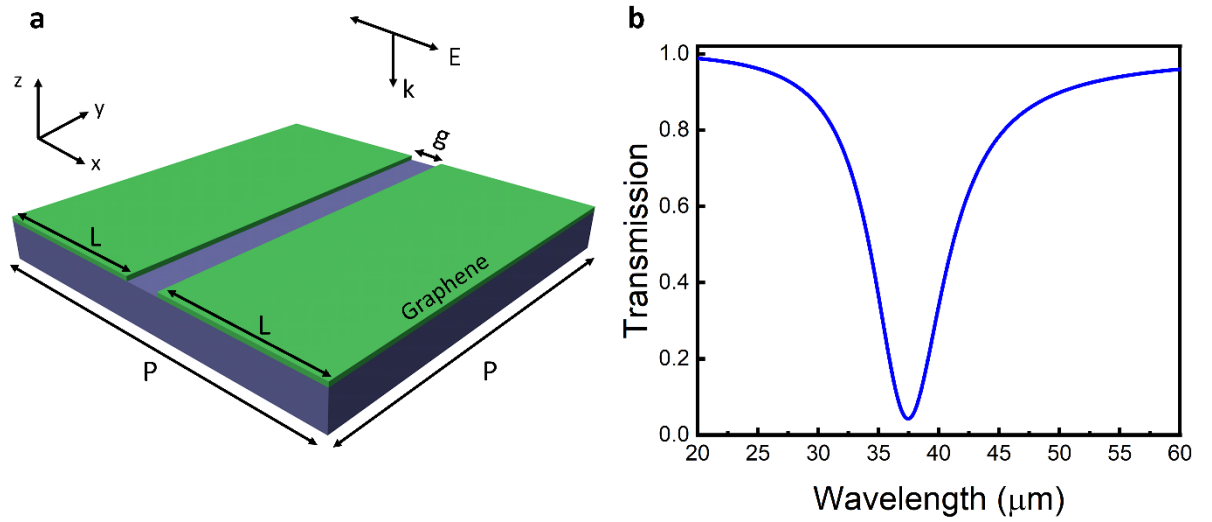


Figure 1. (a) The perspective view of a graphene-based biosensor. L refers to the size of the graphene plate, g to the gap, and P to the single-cell period. (b) Transmission signal graph of graphene biosensor ($g=40$ nm, $Ef=0.4$ eV, $\tau=0.5$).

Graphene is modeled using the Kubo formula in the computational study carried out to investigate the optical properties of the suggested single-layer graphene-based biosensor. To describe the light-matter interaction in metal-based structures, the Drude (and later Lorentz) model is used, which describes in a simple and intuitive way how electrons are transported, and this model underlies the definition of electrical permittivity [19]. In graphene-based structures, this definition is made using the Kubo formula and the isotropic surface conductivity of graphene is expressed as intra-band and inter-band transitions (Eq-1) [20]. This model allows analysis of the conductivity, permeability, chemical potential, plasma frequency, and relaxation time of graphene.

$$\sigma = \sigma_{\text{int } ra}(\omega, \mu_c, \Gamma, T) + \sigma_{\text{int } er}(\omega, \mu_c, \Gamma, T) \quad (1)$$

According to Equation 1, graphene's conductivity depends on the light's energy and the electron-hole pair [20]. Graphene's extraordinary properties can be modified depending on external factors. Particularly, the application of electrostatic fields can change graphene's electronic structure, influencing the antenna resonance mode. Additionally, changes in the relaxation time determined by conductivity affect the optical response. The surface conductivity of graphene based on the Kubo formula is shown in Equations 2 and 3.

$$\sigma_{\text{int } ra}(\omega, \mu_c, \Gamma, T) = i \frac{e^2 k_B T}{\pi \hbar^2 (\omega + 2i\Gamma)} \left(\frac{\mu_c}{k_B T} + 2 \ln \left(e^{-\frac{\mu_c}{\hbar k_B T}} + 1 \right) \right) \quad (2)$$

$$\sigma_{\text{int } er}(\omega, \mu_c, \Gamma, T) = i \frac{e^2}{4\pi \hbar} \ln \frac{2|\mu_c| - (\omega + 2i\Gamma)\hbar}{2|\mu_c| + (\omega + 2i\Gamma)\hbar} \quad (3)$$

Here, μ_c represents the chemical potential, Γ is the scattering rate, T is temperature, e is the electron charge, $\hbar = h/2\pi$ is the reduced Planck's constant, and k_B is the Boltzmann constant. Figure 2 shows the electrical field and charge distribution graphs of the graphene-based biosensor operating in transmission resonance mode. The change in the electric field and charge density along the slit on the single-layer graphene structure showed a distinct behavior. The structure where the electric field distribution is studied in Figure 2a shows that the field distribution along the slit is severely restricted, whereas the field distribution along the left and right graphene plates is significantly decreased. Graphene plasmons evolving across the gap can explain the effect of confining this field on the gap. Figure 2b shows the charge distribution graph along the slit. This graph illustrates how the oscillation of oppositely charged

plasmons at the left and right borders of the slit results in a dipolar charge distribution. This dipolar effect spread strongly across the slit and strengthened the spectral response. In Figure 2c, the electric field effect developing along the slit of the graphene-based biosensor is shown along the z axis. This graph demonstrates the electric field's concentration at the slit's boundaries, providing support for Figure 2a. These physical concepts provide an understanding of the biosensor's strong resonant transmission mode.

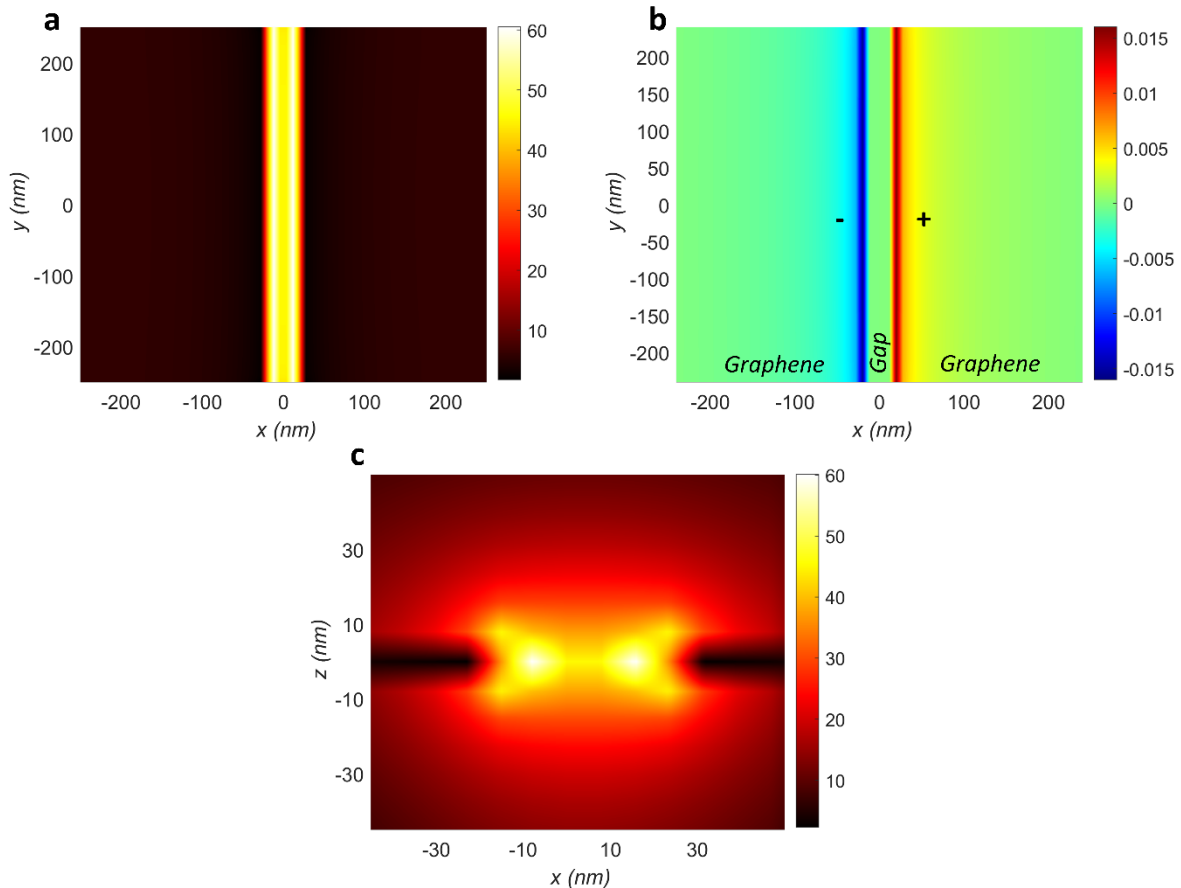


Figure 2. (a) The electric field developing in the graphene slit (gap) is shown in the x-y plane. (b) Charge distribution graph in which the dipole distribution occurs around the graphene slit (gap). (c) Representation of the electric field in the slit in the x-z plane.

Figure 3 demonstrates how altering the slit width in the suggested graphene-based biosensor affects the transmission resonance mode. It has been observed that the resonance mode of the transmission signal shifts to lower wavelengths as the gap between graphene plates increases. This effect in the resonance mode can be explained as an effect of the spatial distribution of graphene plasmons. Another effect is the bandwidth change in the resonant signal with increasing slit width. As the slit width increased, the bandwidth of the resonance mode decreased. Figure 3b uses a scatter plot to further investigate the shift in resonant transmission modes from Figure 3a. This graph indicates that a bigger resonance peak shift was initially produced by increasing the slit width, but that the resonance peak shift decreased as the slit width reached the threshold value. The wide-area dispersion of graphene plasmons is observed to continue at a certain rate, and the effect shown here is compatible with the effects reported in the relevant studies [21], [22]. The numerical analyses presented here illustrate how the size of the split between graphene plates affects the resonance mode, which allows for the optimization of this effect.

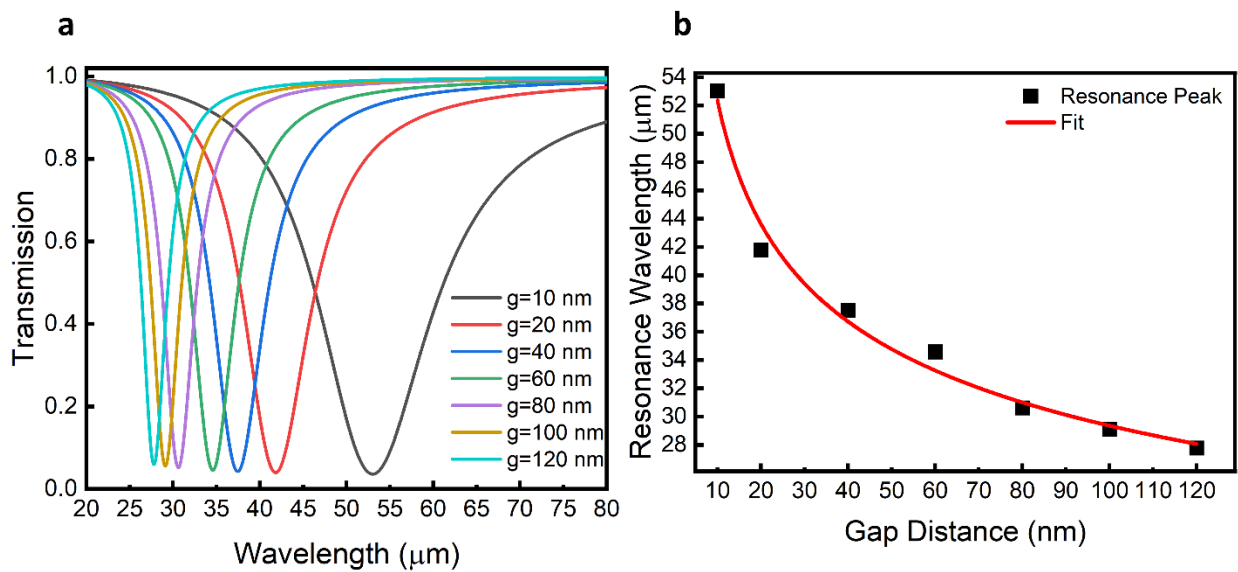


Figure 3. (a) The resonance mode is demonstrated to shift to various wavelengths in response to variations in the gap width(g). (b) The resonance wavelength variation as a function of slit width is demonstrated.

Figure 4 examines how variations in the Fermi energy level affect the resonance wavelength and transmission rate of the graphene-based biosensor. In Figure 4a, the Fermi energy level varied in 0.1 eV increments between 0.1 eV and 0.7 eV, and the signal underwent a blue shift as the Fermi energy level increased. Furthermore, at 0.1 eV energy level, the transmission rate was approximately 75%, but at 0.7 eV energy level, it increased to approximately 99%. The strong interaction in graphene plasmons due to the increase in the charge carrier density of graphene explains this increase. The increase in the transported charge density allows electrostatic gating, shifting the signal to lower wavelengths, increasing the transmission rate and reducing the bandwidth. Figure 4b is illustrated in order to more clearly analyze the effect of this change in the Fermi energy level on the wavelength shift. This graph indicates that while the growing charge density resulting from an increase in Fermi energy level initially exhibited a dramatic wavelength shortening tendency, as it approached the limit values of the graphene charge carrier, it began to exhibit a decreasing trend. This negative correlation between the Fermi energy level and the wavelength explains that graphene plasmons oscillate more strongly and the wavelength becomes shorter with the increase in the fermi energy level. Because greater charges correspond in higher electron density, which expands the space that the graphene layer can enclose. The primary benefit of this is that its static tunability eliminates the need for remanufacturing, allowing it to be utilized in differentiable applications. Thanks to its electrical tunability without changing the physical structure, it can suit different requirements and be integrated into different systems. In addition, changing the Fermi energy can improve the performance of graphene-based sensors and transistors by adjusting the electron transition path. While electrically non-tunable devices require extensive materials for different functions, an electrically tunable graphene-based sensor has a flexible application capability without the need for material changes. This results in a highly flexible tunable sensor platform that can achieve resonance modes at different wavelengths without the need for re-fabrication. In addition to increasing the electrical and optoelectronic flexibility of the sensor, it also eliminates the additional cost burden arising from refabrication.

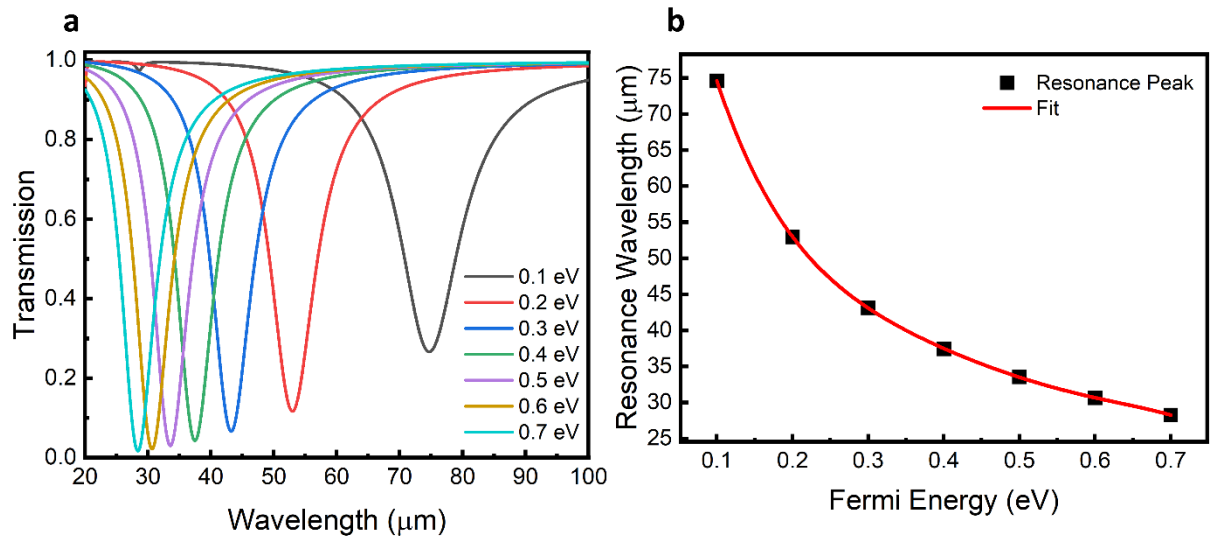


Figure 4. (a) The change in resonance mode due to gradually changing the Fermi energy level. (b) The tendency of the Fermi energy level to switch all resonance modes

Electron mobility is one of the most significant characteristics of graphene. The interaction between electron mobility and chemical potential depends on the relaxation dynamics of electrons within the unique two-dimensional structure of graphene. There is a mean time during the movement of electrons in graphene caused by collisions or scattering. This time indicates the resistance to the mobility of electrons in graphene and the elapsed time. Figure 5a clearly shows that despite the varying relaxation time, the transmission resonance peak remains at the same wavelength. Figure 5b illustrates the effect of changing relaxation time on the transmission percentage. The decreasing carrier density reduces collective oscillations, pulling the transmission rate down from 96% to 74%.

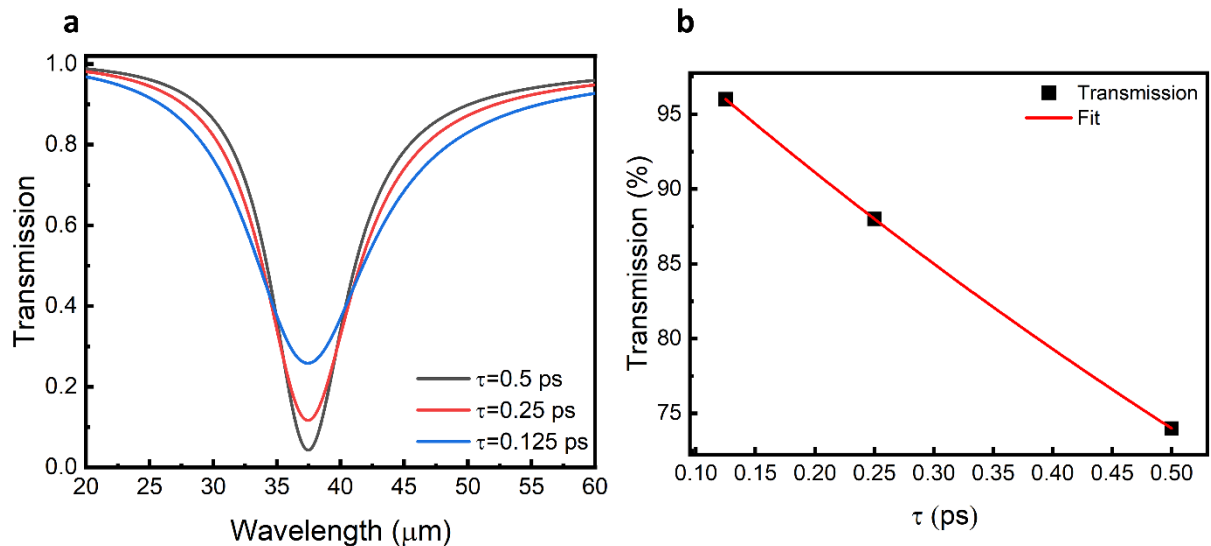


Figure 5. (a) The effect of relaxation time on resonance mode. (b) The variation in transmission strength as a function of relaxation time is demonstrated.

Finally, the sensitivity of the sensor to biomolecular detection was examined. Figure 6a shows the response of the graphene structure with a gap to the changing refractive index of the medium in terms of the transmission resonance mode. In this instance, the medium's refractive index (RI) was changed from 1 to 2, which allowed for the analysis of the transmission spectrum. The characteristic shift of the transmission resonance mode towards longer wavelengths is noticed when RI values grow. This change

affects the coupling conditions of plasmonic excitations and is a direct result of the dielectric shift in the environment surrounding graphene. The increase in the refractive index on the sensor surface is an indicator of an increase in density, and with this increase, a shift to longer wavelengths occurs in order to maintain the resonance mode. The relationship between an increase in refractive index and a rise in resonance wavelength is graphically depicted in Figure 6b. The graph indicates that there is a linear rise in behavior for the 11 points that were obtained in 0.1 increments from $n=1$ to $n=2$. The graph, which is represented by the equation $y=9.535x+27.44$, demonstrates that the wavelength increases linearly with each unit change in RI values. The sensitivity of biosensors can be expressed as a function between the refractive index change per unit and the resonance wavelength change. The sensitivity of the biosensor proposed in this study is computed and expressed with the formula $S=\Delta\lambda/\Delta n$. As a result, 6282 nm/RIU was determined to be the sensor's sensitivity based on the resonance mode caused by $n=1$ refractive index and the resonance mode variation caused by $n=1.1$ refractive index. The sensor sensitivity was computed and the wavelength magnitudes based on the resonant mode peaks were established during this measurement. The graph in Figure 6b shows the linear increase of each point and proves that the sensor will show similar sensitivity at all increments. This level of sensitivity is very sensitive and can be used in biosensing applications.

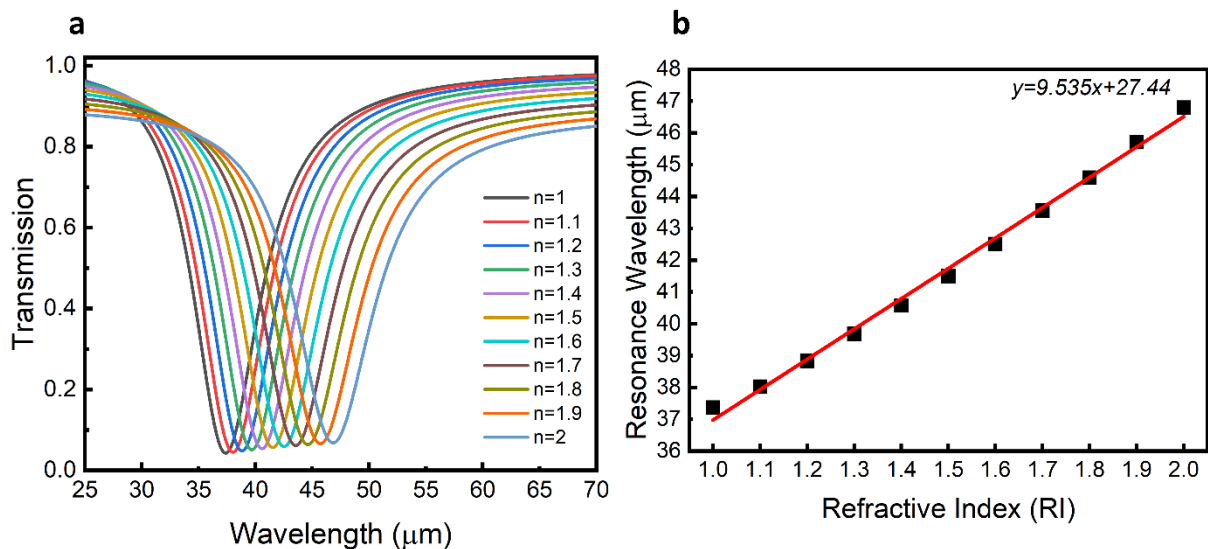


Figure 6. (a) The spectral response of graphene sensor for varying refractive index. (b) The linear relation between the resonance mode of the sensor and the change in refractive index surrounding it.

Table 1 shows recent plasmonic biosensors along with sensor types, materials, and sensitivity data. Sensitivity conditions for biosensors have a direct impact on the sensor's accuracy of detection. Especially for label-free sensing, measuring the resonance mode response due to different refractive indices determines the sensitivity [[23], [24], [25], [26], [27], [28], [29], [30]]. In the literature, metal-based biosensors have been shown to achieve sensitivity rates as high as 2610 nm/RIU. However, biosensors with these metal structures have serious disadvantages due to their cost, difficulty in production and oxidation by bioanalytes. In addition, the high ohmic loss of metals limits the propagation and reduces the impact of evolving plasmons. They also require remanufacturing after they are built since they cannot be statically adjusted to different resonance modes. On the other hand, graphene offers benefits including strong field restrictions, minimal losses, and low prices because of its exceptional electrical and optical properties. These benefits have led to discussions on graphene-based sensors and the proposal of highly sensitive sensors like 2900 nm/RIU. The graphene-based biosensor proposed in this article has been shown to have a stronger detection ability compared to similar studies, showing a sensitivity rate of 6282 nm/RIU. In addition to the advantage of high sensitivity, the proposed biosensor structure also offers advantages such as low cost and static tunability. In this way, it becomes easier to

integrate into different sensing applications that require different resonance modes.

The fabrication of this graphene-based biosensor, which exhibits strong detection ability in numerical analysis, is carried out by following several different nanofabrication steps. Graphene is grown using methods such as chemical vapor deposition (CVD) and can be transferred to any desired surface. Graphene grown on a copper foil is transferred to the surface with a support layer such as polymethyl methacrylate (PMMA) in order to be transferred safely. Then, the copper foil on the surface is removed using Ferric Chloride solid. Single-layer graphene transfer is achieved by cleaning the dissolved PMMA layer. Electron beam lithography (EBL) and reactive ion etching (RIE) methods can be used to create a 40 nm wide slit in the middle of the monolayer graphene layer on the surface. The surface is coated with EBL positive resistivity PMMA, baked, and the 40 nm wide gap is subjected to electron bombardment. Then, the chip is kept in Methyl isobutyl ketone (MIBK) liquid and the area exposed to the electron beam is developed. The sensor is immersed in IPA and rinsed, and a 40 nm wide slit is opened up to the graphene layer. Subsequently, RIE is utilized to etch the graphene layer, creating a precise 40 nm wide strip.

Table 1. The sensitivity values obtained from recent literature articles

	Year	Sensor structure type	Material	S (nm/RIU)
[23]	2016	Plasmonic Au Sensor	Au	623
[24]	2017	Plasmonic Ag Sensor	Ag	2610
[25]	2018	Metal-insulator-metal (MIM) waveguide coupled with concentric double rings resonator (CDRR)	Ag	1060
[26]	2019	Plasmonic Graphene Ribbon	Graphene	2900
[27]	2020	Plasmonic Ag Sensor	Ag	1380
[28]	2021	Plasmonic Sensor	Si/Au	1320
[29]	2022	Plasmonic Perfect Absorber	LiNbO3/Graphene/Au	981
[30]	2023	Plasmonic Ring Resonator	Si/Graphene	2200
This work	2024	Plasmonic Graphene Sensor	SiO2/Graphene	6282

4. CONCLUSIONS

In this paper, a graphene-based biosensor is proposed to eliminate the disadvantages of metal-based plasmonic biosensors. The graphene monolayer is placed on the substrate and a cavity is formed in the center of this layer. This graphene cavity has a high transmission resonance mode of 96.2% due to the limited propagation of graphene plasmons around it. The excellent electrical and optical capabilities of graphene have been exploited with this evolving resonance mode. The effects of the width of the graphene cavity and the relaxation time of the graphene on the transmission resonance mode are discussed in detail and the optimum transmission mode is determined. In addition, the electrical tunability of graphene is exploited to show that the antenna shifts to different resonant modes at varying fermi energy levels, resulting in static tunability. The variation of the sensor resonance mode against the changing refractive index on the sensor surface is thoroughly examined after the optimal transmission

mode with all of these parameters has been found. The results show that the sensor has a high sensitivity of 6282 nm/RIU.

Declaration of Ethical Standards

Authors declare to comply with all ethical guidelines including authorship, citation, data reporting, and publishing original research.

Declaration of Competing Interest

The authors declare that they have no known competing financial interests or personal relationships that could have appeared to influence the work reported in this paper.

Funding / Acknowledgements

No funding is available for this research.

Data Availability

Data will be made available on request.

5. REFERENCES

- [1] A. Jarahi Khameneh *et al.*, "Trends in electrochemical biosensors for the early diagnosis of breast cancer through the detection of relevant biomarkers," *Chemical Physics Impact*, vol. 8, no. September 2023, p. 100425, 2024, doi: 10.1016/j.chphi.2023.100425.
- [2] S. Mummareddy, S. Pradhan, A. K. Narasimhan, and A. Natarajan, "On demand biosensors for early diagnosis of cancer and immune checkpoints blockade therapy monitoring from liquid biopsy," *Biosensors (Basel)*, vol. 11, no. 12, 2021, doi: 10.3390/bios11120500.
- [3] J. Yoon, M. Shin, T. Lee, and J. W. Choi, "Highly sensitive biosensors based on biomolecules and functional nanomaterials depending on the types of nanomaterials: A perspective review," *Materials*, vol. 13, no. 2, pp. 1–21, 2020, doi: 10.3390/ma13020299.
- [4] D. Bhatia, S. Paul, T. Acharjee, and S. S. Ramachairy, "Biosensors and their widespread impact on human health," *Sensors International*, vol. 5, no. July 2023, p. 100257, 2024, doi: 10.1016/j.sintl.2023.100257.
- [5] N. Bontempi *et al.*, "Highly sensitive biosensors based on all-dielectric nanoresonators," *Nanoscale*, vol. 9, no. 15, pp. 4972–4980, 2017, doi: 10.1039/c6nr07904k.
- [6] A. A. Smith, R. Li, and Z. T. H. Tse, "Reshaping healthcare with wearable biosensors," *Sci Rep*, vol. 13, no. 1, pp. 1–16, 2023, doi: 10.1038/s41598-022-26951-z.
- [7] M. E. Hamza, M. A. Othman, and M. A. Swillam, "Plasmonic Biosensors: Review," *Biology (Basel)*, vol. 11, no. 5, 2022, doi: 10.3390/biology11050621.
- [8] H. Yu, Y. Peng, Y. Yang, and Z. Y. Li, "Plasmon-enhanced light–matter interactions and applications," *NPJ Comput Mater*, vol. 5, no. 1, pp. 1–14, 2019, doi: 10.1038/s41524-019-0184-1.
- [9] H. A. Elsayed *et al.*, "High-performance biosensors based on angular plasmonic of a multilayer design: new materials for enhancing sensitivity of one-dimensional designs," *RSC Adv*, vol. 14, no. 11, pp. 7877–7890, 2024, doi: 10.1039/d3ra08731j.
- [10] Y. V. Stebunov, D. I. Yakubovsky, D. Y. Fedyanin, A. V. Arsenin, and V. S. Volkov, "Superior Sensitivity of Copper-Based Plasmonic Biosensors," *Langmuir*, vol. 34, no. 15, pp. 4681–4687, 2018, doi: 10.1021/acs.langmuir.8b00276.

- [11] M. E. E. Alahi, M. I. Rizu, F. W. Tina, Z. Huang, A. Nag, and N. Afsarimanesh, "Recent Advancements in Graphene-Based Implantable Electrodes for Neural Recording/Stimulation," *Sensors*, vol. 23, no. 24, 2023, doi: 10.3390/s23249911.
- [12] Y. Bai, T. Xu, and X. Zhang, "Graphene-based biosensors for detection of biomarkers," *Micromachines (Basel)*, vol. 11, no. 1, 2020, doi: 10.3390/mi11010060.
- [13] J. Peña-Bahamonde, H. N. Nguyen, S. K. Fanourakis, and D. F. Rodrigues, "Recent advances in graphene-based biosensor technology with applications in life sciences," *J Nanobiotechnology*, vol. 16, no. 1, pp. 1–17, 2018, doi: 10.1186/s12951-018-0400-z.
- [14] V. B. Mbayachi, E. Ndayiragije, T. Sammani, S. Taj, E. R. Mbuta, and A. ullah khan, "Graphene synthesis, characterization and its applications: A review," *Results Chem*, vol. 3, p. 100163, 2021, doi: 10.1016/j.rechem.2021.100163.
- [15] H. N. K. AL-Salman *et al.*, "Graphene oxide-based biosensors for detection of lung cancer: A review," *Results Chem*, vol. 7, no. November 2023, p. 101300, 2024, doi: 10.1016/j.rechem.2023.101300.
- [16] M. T. Hwang *et al.*, "Ultrasensitive detection of nucleic acids using deformed graphene channel field effect biosensors," *Nat Commun*, vol. 11, no. 1, 2020, doi: 10.1038/s41467-020-15330-9.
- [17] D. L. P. and M. F. Ashok K. Sood, Isaac Lund, Yash R. Puri, Harry Efstathiadis, Pradeep Haldar, Nibir K. Dhar, Jay Lewis, Madan Dubey, Eugene Zakar, Priyalal Wijewarnasuriya, "Review of Graphene Technology and Its Applications for Electronic Devices," in *Graphene - New Trends and Developments*, 2015.
- [18] S. H. Oh *et al.*, "Nanophotonic biosensors harnessing van der Waals materials," *Nat Commun*, vol. 12, no. 1, pp. 1–18, 2021, doi: 10.1038/s41467-021-23564-4.
- [19] A. Alabastri *et al.*, "Molding of plasmonic resonances in metallic nanostructures: Dependence of the non-linear electric permittivity on system size and temperature," *Materials*, vol. 6, no. 11, pp. 4879–4910, 2013, doi: 10.3390/ma6114879.
- [20] S. Cynthia, R. Ahmed, S. Islam, K. Ali, and M. Hossain, "Graphene based hyperbolic metamaterial for tunable mid-infrared biosensing," *RSC Adv*, vol. 11, no. 14, pp. 7938–7945, 2021, doi: 10.1039/d0ra09781k.
- [21] R. B. Hwang, "A theoretical design of evanescent wave biosensors based on gate-controlled graphene surface plasmon resonance," *Sci Rep*, vol. 11, no. 1, pp. 1–10, 2021, doi: 10.1038/s41598-021-81595-9.
- [22] Y. Wu, Q. Nie, C. Tang, B. Yan, F. Liu, and M. Zhu, "Bandwidth tunability of graphene absorption enhancement by hybridization of delocalized surface plasmon polaritons and localized magnetic plasmons," *Discover Nano*, vol. 19, no. 1, 2024, doi: 10.1186/s11671-024-03961-6.
- [23] Y. Liang, M. Lu, S. Chu, L. Li, and W. Peng, "Tunable Plasmonic Resonances in the Hexagonal Nanoarrays of Annular Aperture for Biosensing," *Plasmonics*, vol. 11, no. 1, pp. 205–212, 2016, doi: 10.1007/s11468-015-0041-0.
- [24] M. R. Rakhshani and M. A. Mansouri-Birjandi, "Utilizing the Metallic Nano-Rods in Hexagonal Configuration to Enhance Sensitivity of the Plasmonic Racetrack Resonator in Sensing Application," *Plasmonics*, vol. 12, no. 4, pp. 999–1006, 2017, doi: 10.1007/s11468-016-0351-x.
- [25] Z. Zhang *et al.*, "Plasmonic refractive index sensor with high figure of merit based on concentric-rings resonator," *Sensors (Switzerland)*, vol. 18, no. 1, 2018, doi: 10.3390/s18010116.
- [26] H. Yang *et al.*, "High-sensitivity plasmonics biosensor based on graphene ribbon arrays," *2019 7th International Conference on Information, Communication and Networks, ICICN 2019*, pp. 105–108, 2019, doi: 10.1109/ICICN.2019.8834950.
- [27] M. R. Rakhshani, "Optical refractive index sensor with two plasmonic double-square resonators for simultaneous sensing of human blood groups," *Photonics Nanostruct*, vol. 39, no. August 2019, p. 100768, 2020, doi: 10.1016/j.photonics.2020.100768.
- [28] L. Hajshahvaladi, H. Kaatuzian, and M. Danaie, "A high-sensitivity refractive index biosensor based on Si nanorings coupled to plasmonic nanohole arrays for glucose detection in water

- solution," *Opt Commun*, vol. 502, no. August 2021, p. 127421, 2022, doi: 10.1016/j.optcom.2021.127421.
- [29] M. Irfan, Y. Khan, A. U. Rehman, M. A. Butt, S. N. Khonina, and N. L. Kazanskiy, "Plasmonic Refractive Index and Temperature Sensor Based on Graphene and LiNbO₃," *Sensors*, vol. 22, no. 20, 2022, doi: 10.3390/s22207790.
- [30] S. K. Patel, J. Surve, J. Parmar, K. Aliqab, M. Alsharari, and A. Armghan, "SARS-CoV-2 detecting rapid metasurface-based sensor," *Diam Relat Mater*, vol. 132, no. November 2022, p. 109644, 2023, doi: 10.1016/j.diamond.2022.109644.